Hepatitis C Virus Disrupts Annexin 5-Mediated Occludin Integrity through Downregulation of Protein Kinase Cα (PKCα) and PKCη Expression, Thereby Promoting Viral Propagation

Takayuki Abe,[a] Yuki Marutani,[a] Lin Deng,[a] Chieko Matsui,[a] Masayoshi Fukasawa,[b] Ryosuke Suzuki,[c] Takaji Wakita,[c] Yoshiharu Matsuura,[d,e] Ikuo Shoji[a]

[a]Division of Infectious Disease Control, Center for Infectious Diseases, Kobe University Graduate School of Medicine, Kobe, Japan

[b]Department of Biochemistry and Cell Biology, National Institute of Infectious Diseases, Tokyo, Japan

[c]Department of Virology II, National Institute of Infectious Diseases, Tokyo, Japan

[d]Center for Infectious Diseases Education and Research (CiDER), Osaka University, Osaka, Japan

[e]Laboratory of Virus Control, Research Institute for Microbial Diseases (RIMD), Osaka University, Osaka, Japan

ABSTRACT Annexins (ANXs) comprise a family of calcium- and phospholipid-binding proteins and are implicated in the hepatitis C virus (HCV) life cycle. Here, we demonstrate a novel role of ANX5 in the HCV life cycle. Comparative analysis by quantitative PCR in human hepatoma cells revealed that ANX2, ANX4, and ANX5 were highly expressed among the ANX family proteins. Knockdown of ANX5 mRNA resulted in marked enhancement of HCV RNA replication but had no effect on either HCV translation or assembly. Using the HCV pseudoparticle (HCVpp) system, we observed enhancement of HCVpp infectivity in ANX5 knockdown Huh-7OK1 cells, suggesting that ANX5 is involved in suppression of HCV entry. Additionally, we observed that subcellular localizations of tight-junction proteins, such as claudin 1 (CLDN1) and occludin (OCLN), were disrupted in the ANX5 knockdown cells. It was reported that HCV infection was facilitated by disruption of OCLN distribution and that proper distribution of OCLN was regulated by its phosphorylation. Knockdown of ANX5 resulted in a decrease of OCLN phosphorylation, thereby disrupting OCLN distribution and HCV infection. Further analysis revealed that protein kinase C (PKC) isoforms, including PKCα and PKCη, play important roles in the regulation of ANX5-mediated phosphorylation and distribution of OCLN and in the restriction of HCV infection. HCV infection reduced OCLN phosphorylation through the downregulation of PKCα and PKCη expression. Taken together, these results suggest that ANX5, PKCα, and PKCη contribute to restriction of HCV infection by regulating OCLN integrity. We propose a model that HCV disrupts ANX5-mediated OCLN integrity through downregulation of PKCα and PKCη expression, thereby promoting HCV propagation.

IMPORTANCE Host cells have evolved host defense machinery to restrict viral infection. However, viruses have evolved counteracting strategies to achieve their infection. In the present study, we obtained results suggesting that ANX5 and PKC isoforms, including PKCα and PKCη, contribute to suppression of HCV infection by regulating the integrity of OCLN. The disruption of OCLN integrity increased HCV infection. We also found that HCV disrupts ANX5-mediated OCLN integrity through downregulation of PKCα and PKCη expression, thereby promoting viral infection. We propose that HCV disrupts ANX5-mediated OCLN integrity to establish a persistent infection. The disruption of tight-junction assembly may play important roles in the progression of HCV-related liver diseases.

KEYWORDS hepatitis C virus, annexin 5, protein kinase C, occludin, tight junction

Hepatitis C virus (HCV) infection is a leading cause of chronic hepatitis, liver cirrhosis, and hepatocellular carcinoma and represents a major public health burden worldwide. HCV is an enveloped, single-stranded positive-sense RNA virus classified into the *Hepacivirus* genus of the *Flaviviridae* family. The HCV genome consists of 9.6-kb RNA encoding a single polyprotein which is processed by viral proteases and cellular signalases to produce three structural proteins (core, E1, and E2) and seven nonstructural (NS) proteins (p7, NS2, NS3, NS4A, NS4B, NS5A, and NS5B) (1). Replication of the viral RNA occurs on the endoplasmic reticulum (ER)-derived double-membrane vesicles (termed the membranous web) and requires the participation of NS2 to NS5B together with cellular host factors (2–4).

Accumulating evidence suggests that a large number of host factors associate with HCV proteins at the membranous web to permit efficient viral replication (4, 5). Quantitative proteomics analysis for viral replication complexes purified from HCV replicon cells has revealed that annexins (ANXs), a family of calcium-dependent, phospholipid-binding proteins, consist of the host factors required for HCV infection (6, 7). ANX2, one of the ANXs highly associated with the HCV life cycle, is specifically recruited by NS5A protein at the membranous web to promote the viral assembly process (6). ANX2 functions as a scaffold protein to stabilize the structural organization of the membranous web, which consists of the lipid raft microdomain, thereby promoting HCV replication (7). Solbak and colleagues (8) reported that ANX2 directly binds to NS5B protein and results in a decrease of the affinity for the allosteric inhibitor filibuvir, suggesting that ANX2 affects the treatment of HCV infection. The membranous web and the cytosolic lipid droplets (LDs) provide the sites of HCV assembly. It has been reported that ANX3 is recruited to a lipid droplet compartment in the HCV-infected cells to promote viral particle production through the association of viral envelope E2 with apolipoprotein E (ApoE) (9). Despite these research contributions, the mechanistic details of the ANX proteins in the HCV life cycle remain to be elucidated.

ANX5 has been suggested to mediate signal transduction, cell cycle regulation, membrane fusion, and membrane organization (10). In addition, the binding of ANX5 to phosphatidylserine (PS) accounts for detection of apoptotic cells (11). In this study, we investigated a role of ANX5 in the assembly of tight junctions (TJs) and regulation of HCV propagation. The TJs form the cell-cell junctions that are impermeable to the majority of soluble molecules (e.g., ions and water) between the two sides of the epithelium. Recently, various novel aspects of TJs have been reported, including their involvement in signal transduction and innate immunity (12). Protein kinase C (PKC)-mediated occludin (OCLN) phosphorylation plays a crucial role in the regulation of TJ assembly (13–15). HCV infectivity was facilitated by disruption of OCLN distribution (16). The physiological role of ANX5 in the regulation of TJ assembly to combat HCV infection is still ill defined.

Here, we demonstrate that ANX5 and PKC isoforms, including PKCα and PKCη, contribute to suppression of HCV infection by regulating the integrity of OCLN. We further demonstrate that HCV disrupts ANX5-mediated OCLN integrity through the downregulation of PKCα and PKCη expression, thereby promoting viral propagation.

RESULTS

ANX5 negatively regulates HCV RNA replication. To determine the possible involvement of novel ANXs in the HCV life cycle, we analyzed expression profiles of ANXs in Huh-7.5 cells. Quantitative PCR (qPCR) analysis revealed high levels of mRNA expression of ANX4 and ANX5 as well as ANX2 in Huh-7.5 cells (Fig. 1A).

To investigate whether these ANXs are involved in HCV RNA replication, we performed small interfering RNA (siRNA)-mediated knockdown of ANXs in HCV subgenomic replicon (SGR) cells (1b, Con1, 9-13 clone). The knockdown efficiency was confirmed by immunoblotting and qPCR, demonstrating that each of the ANXs (Fig. 1B and C) were sufficiently knocked down (by approximately 80%). Interestingly, the knockdown of ANX5 resulted in marked enhancement of the expression of both NS5A proteins and HCV RNA levels in the HCV SGR cells compared to those in the cells transfected with
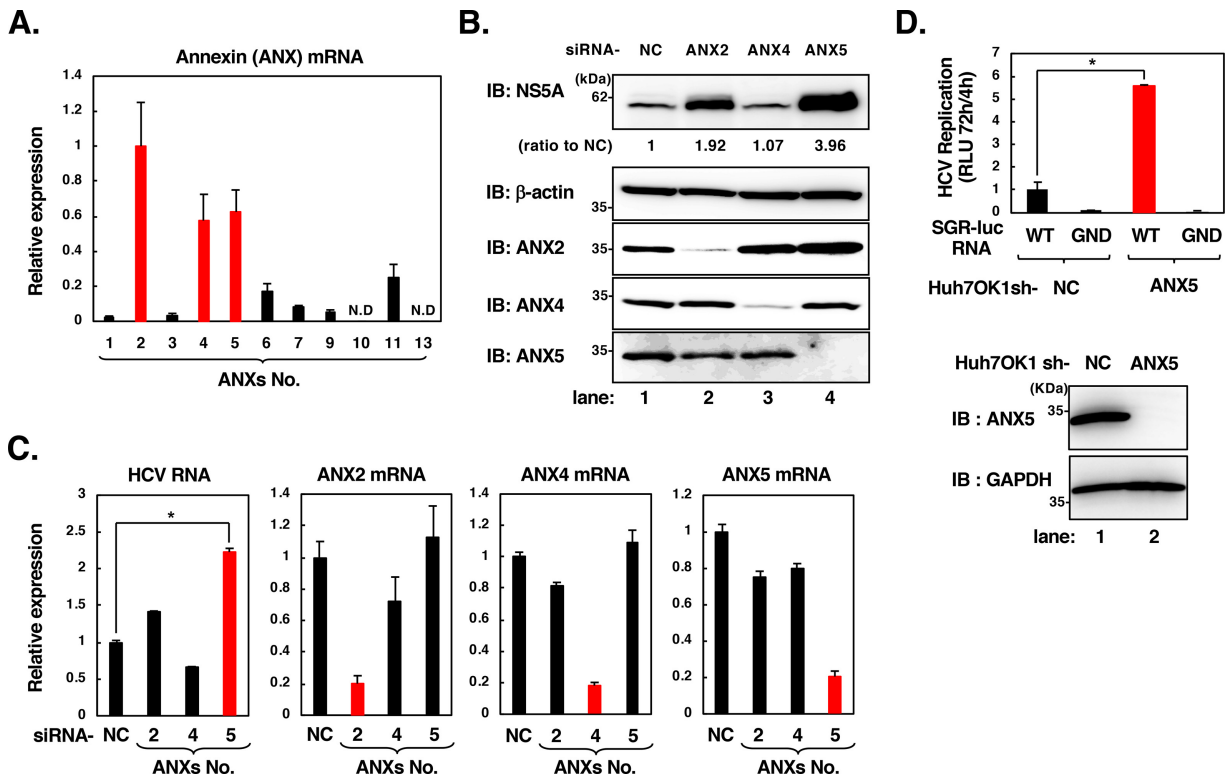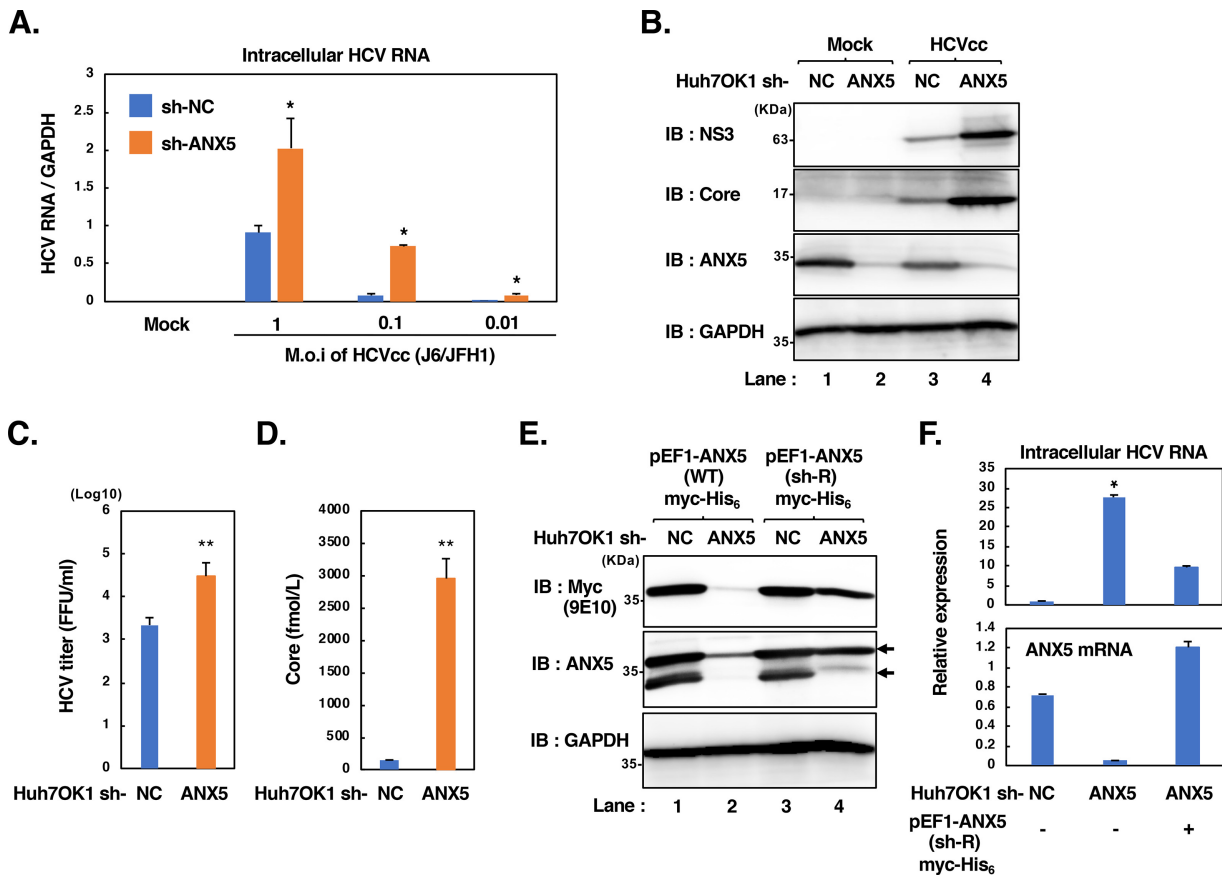
FIG 1 ANX5 negatively regulates HCV RNA replication. (A) Total RNA was extracted from Huh-7.5 cells, and mRNA levels of annexins (ANXs) were measured by real-time PCR. N.D, not detected. (B) HCV subgenomic replicon (SGR) cells carrying genotype 1b (Con1, 9-13 clone) were transfected with 50 nM synthetic siRNA targeted to negative control (NC), ANX2, ANX4, or ANX5 and cultured for 72 h. The cell lysates were subjected to immunoblotting (IB) with the indicated antibodies. The band intensities of NS5A were determined by using ImageQuant TL software (version 7). (C) HCV SGR cells were transfected with siRNA targeted to NC, ANX2, ANX4, or ANX5. Real-time qPCR was performed with the indicated specific primers. Results are the mean values of triplicates $\pm$ SDs. Data from the real-time PCR were normalized to the amount of GAPDH mRNA. (D) Huh-7OK1-sh-NC and Huh-7OK1-sh-ANX5 cells were electroporated with either HCV SGR RNA derived from the Con1 wild type (WT) or a replication-defective mutant (GND), which possess a firefly luciferase gene (SGR-Luc RNA). At 72 h after electroporation of HCV SGR RNA, the cells were lysed and subjected to a luciferase assay. The luciferase activity measured 4 h after electroporation was used to normalize the input RNA. Results are shown as mean values of triplicates $\pm$ SDs of normalized relative light units (RLUs) at 72 h after electroporation ($n = 3$ biological replicates). *, $P < 0.05$ versus the results for cells transduced with Huh-7OK1-sh-NC cells. The expression levels of endogenous ANX5 and GAPDH were determined by IB (bottom). The Western blots are representative of three independent experiments.

negative-control (NC) siRNA (Fig. 1B, top, compare lane 1 with lane 4; Fig. 1C, first graph). The knockdown of ANX4 had no effect on HCV RNA replication (Fig. 1C, first graph). The knockdown of ANX2 resulted in an increase of both NS5A proteins and HCV RNA expression (Fig. 1B, top, compare lane 1 with lane 2; Fig. 1C, first graph). These results suggest that ANX2 and ANX5 are involved in the suppression of HCV RNA replication. Because the knockdown of ANX5 had a greater impact on HCV RNA replication than the knockdown of ANX2 (Fig. 1C), we focused on ANX5 in the following study.

To further clarify the role of ANX5 in HCV RNA replication, we established cells stably expressing short hairpin RNA (shRNA) targeted to ANX5 (sh-ANX5) on the basis of a human hepatoma cell line with high permissiveness for HCV infection (Huh-7OK1). We then electroporated HCV reporter SGR RNA (SGR-Luc RNA) into the cells to evaluate the viral replication by measuring the luciferase activity. Immunoblot analysis confirmed that ANX5 expression was undetectable in the sh-ANX5 cells (Fig. 1D, bottom, lane 2). The reporter activity of HCV-SGR-Luc RNA in the sh-ANX5 cells was significantly enhanced compared to that in the sh-NC cells (Fig. 1D, top). These results suggest that ANX5 negatively regulates HCV RNA replication.

ANX5 negatively regulates HCV propagation. To further examine the role of ANX5 in HCV propagation, we infected sh-NC Huh-7OK1 cells and sh-ANX5 Huh-7OK1 cells with cell culture-adapted HCV (HCVcc) J6/JFH1 and measured intracellular viral

FIG 2 ANX5 negatively regulates HCV propagation. (A) Huh-7OK1-sh-NC and Huh-7OK1-sh-ANX5 cells were infected with HCVcc J6/JFH1 at a multiplicity of infection (MOI) of 1, 0.1, or 0.01. At 5 days postinoculation, the expression levels of intracellular HCV RNA were determined by real-time PCR. Results are the mean values of triplicates ± SDs ($n = 3$ biological replicates). *, $P < 0.05$ versus the results for the cells the HCVcc-infected Huh-7OK1-sh-NC cells. Data from the real-time PCR were normalized to the amount of GAPDH mRNA. (B to D) Huh-7OK1-sh-NC and Huh-7OK1-sh-ANX5 cells were infected with HCVcc J6/JFH1 at an MOI of 1, 0.1, or 0.01. At 5 days postinoculation, the cell lysates were harvested and subjected to immunoblotting with the indicated antibodies (B). (C and D) Huh-7OK1-sh-NC and Huh-7OK1-sh-ANX5 cells were infected with HCVcc J6/JFH1 at an MOI of 0.1. The extracellular HCV infectivity titers were measured (C). The levels of extracellular core proteins at 5 days postinoculation were quantified by core ELISA (D). Results are the mean values of triplicates ± SDs ($n = 3$ biological replicates). **, $P < 0.01$ versus the results for the HCVcc-infected Huh-7OK1-sh-NC cells. The Western blots are representative of three independent experiments. (E) Huh-7OK1-sh-NC and Huh-7OK1-sh-ANX5 cells were infected with HCVcc J6/JFH1 at an MOI of 0.1. At 2 days postinoculation, the cells were transfected with pEF1-ANX5(WT)-myc-His$_6$ or pEF1-ANX5(sh-R)-myc-His$_6$. Cells were harvested at 72 h after transfection and subjected to immunoblot analysis with the indicated antibodies. The upper and lower arrows indicate an exogenous (ANX5-Myc-His$_6$) and endogenous ANX5, respectively. The Western blots are representative of three independent experiments. (F) Either Huh-7OK1-sh-NC cells or Huh-7OK1-sh-ANX5 cells were infected with HCVcc J6/JFH1 at an MOI of 0.1. At 48 h postinoculation, the cells were transfected with either pEF1-myc-His$_6$ or pEF1-ANX5(sh-R)-myc-His$_6$. Real-time RT-PCR analysis was performed to measure the expression levels of intracellular HCV RNA and ANX5 mRNA at 72 h after transfection. Results are the mean values of triplicates ± SDs ($n = 3$ biological replicates). *, $P < 0.05$ versus the results for the HCVcc-infected Huh-7OK1-sh-NC cells. Data from the real-time RT-PCR were normalized to the amount of GAPDH mRNA.

RNA and viral proteins. We assayed for extracellular viral infectivity titer and extracellular core proteins in the supernatant of the infected cells at 5 days postinoculation. We observed significant enhancement in the intracellular HCV RNA levels (Fig. 2A) and HCV core protein and NS3 protein (Fig. 2B, first and second blots, compare lane 3 with lane 4), the extracellular viral infectivity titers (Fig. 2C), and the extracellular core proteins (Fig. 2D) in the sh-ANX5 cells compared to those in the sh-NC cells. Moreover, to exclude possible off-target effects, we performed rescue experiments. We infected the sh-ANX5 cells with HCVcc J6/JFH1. At 48 h postinoculation, we transfected the cells with a plasmid carrying a C-terminal Myc-His$_6$-tagged ANX5 wobble mutant [pEF1-ANX5-(shR)-myc-His$_6$], which is resistant to sh-ANX5 (Fig. 2E). In accordance with the rescue of ANX5 expression, intracellular HCV RNA levels were decreased in the sh-ANX5 cells transfected with pEF1-ANX5-(shR)-myc-His$_6$ compared to the sh-ANX5 cells
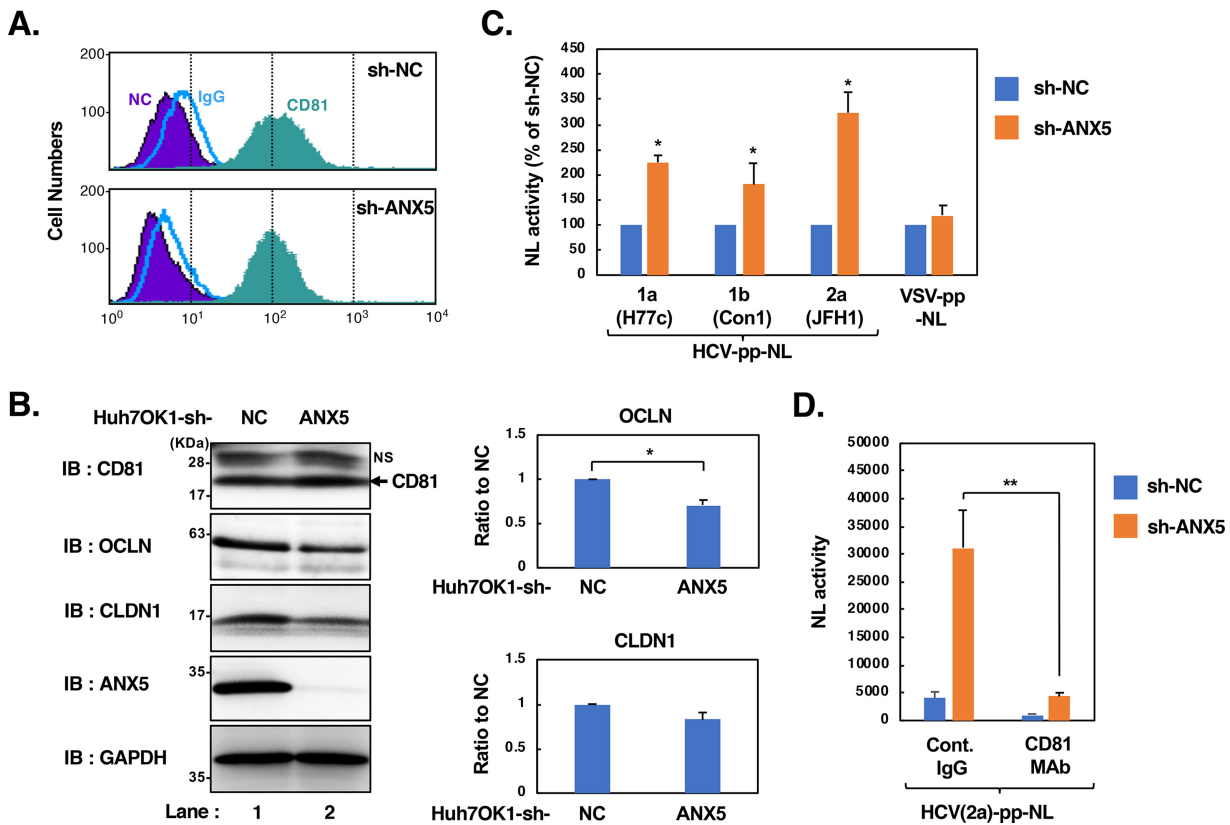
FIG 3 ANX5 negatively regulates HCV entry. (A) The cell surface expression of CD81 on Huh-7OK1-sh-NC and Huh-7OK1-sh-ANX5 cells was determined by flow cytometry. The filled histograms colored purple and green indicate results for unstained negative-control (NC) cells and stained (CD81) cells, respectively. Blue lines indicate results for the isotype control IgG. (B) Cell lysates were prepared from Huh-7OK1-sh-NC and Huh-7OK1-sh-ANX5 cells and subjected to IB with the indicated antibodies. The Western blots are representative of three independent experiments. NS, nonspecific bands. The relative levels of CLDN1 and OCLN expression were quantified by ImageQuant TL software (version 7.0) and are indicated on the right side of the blots. *, $P < 0.05$ versus the results for the Huh-7OK1-sh-NC cells. (C) Huh-7OK1-sh-NC and Huh-7OK1-sh-ANX5 cells were inoculated with HCVpp genotypes (1a [H77c], 1b [Con1], and 2a [JFH1]) or VSVpps. At 3 days postinoculation, the cells were lysed, and the NL activity was measured. Results are the mean values of triplicates $\pm$ SDs ($n = 3$ biological replicates). *, $P < 0.05$ versus the results for the cells inoculated with Huh-7OK1-sh-NC cells. (D) Huh-7OK1-sh-NC and Huh-7OK1-sh-ANX5 cells were pretreated with antibodies against CD81 mouse MAb or isotype control IgG. At 1 h posttreatment, the cells were inoculated with HCVpps from genotype 2a, and the NL activity was measured at 3 days postinoculation. Results are the mean values of triplicates $\pm$ SDs ($n = 3$ biological replicates). **, $P < 0.01$ versus the results for the cells treated with isotype control IgG.

transfected with an empty plasmid (Fig. 2F). These results suggest that ANX5 negatively regulates viral propagation in HCV-infected cells.

ANX5 negatively regulates HCV entry via CD81. Next, to determine whether the other steps of the HCV life cycle are negatively regulated by ANX5, we used an HCV pseudoparticle (HCVpp) system carrying the nanoluciferase (NL) reporter gene to analyze the entry step of HCV infection. Comparative analysis by flow cytometry and immunoblotting revealed that the level of CD81 protein expression in the sh-ANX5 Huh-7OK1 cells was comparable to that in the sh-NC Huh-7OK1 cells (Fig. 3A and B). However, we observed a slight decrease in claudin 1 (CLDN1) and OCLN expression in the sh-ANX5 cells (Fig. 3B, second and third blots, lane 2). These results suggest that aggregation of OCLN and CLDN1 was due to the distribution change rather than the decreased expression. Inoculation of HCVpps derived from genotypes 1a (H77c), 1b (Con1), and 2a (JFH1) resulted in a significant enhancement of NL activity in the sh-ANX5 cells compared to that in sh-NC cells (Fig. 3C), while the NL activity from vesicular stomatitis virus pseudoparticle (VSVpp) inoculation was not significantly different between these two cell lines (Fig. 3C). Moreover, the enhanced NL activity in the sh-ANX5 cells inoculated with HCVpps (2a, JFH1) was significantly decreased by treatment with anti-CD81 monoclonal antibody (MAb) (Fig. 3D). These results suggest that ANX5 negatively regulates HCV entry via CD81.
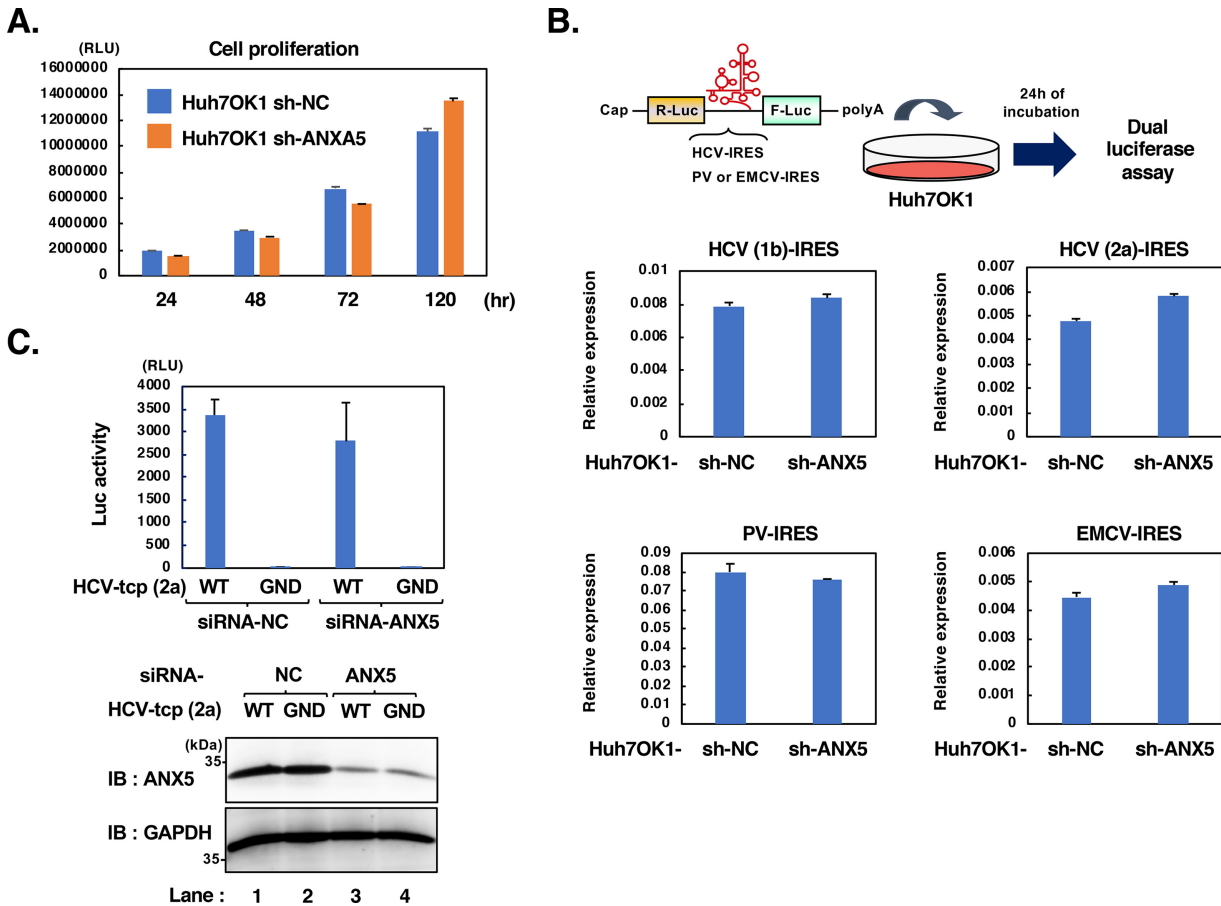
FIG 4 Effect of ANX5 on cell proliferation and different steps of the HCV life cycle. (A) Huh-7OK1-sh-NC and Huh-7OK1-sh-ANXA5 cells were seeded on a 96-well plate at 3×10^3 cells/well and cultured for the indicated durations. The degree of cell proliferation was determined by luminescent cell viability assay. Results are shown as the mean values of triplicates $\pm$ SDs ($n = 3$ biological replicates). (B) Huh-7OK1-sh-NC and Huh-7OK1-sh-ANXA5 cells were transfected with a bicistronic luciferase expression construct (HCV-IRES-Fluc/Cap-Rluc-polyA). At 24 h posttransfection, luciferase activity was determined by dual-luciferase assay. The results are shown as the ratio of IRES-dependent Fluc to the cap-dependent Rluc value. Results are shown as the mean values of triplicates $\pm$ SDs ($n = 3$ biological replicates). (C) The plasmid encoding core-NS2 and the plasmid encoding the bicistronic subgenomic luciferase reporter replicon sequence were cotransfected into the Huh-7.5 cells treated with siRNA-NC or siRNA-ANX5. At 5 days posttransfection, the supernatants, including HCVtcp (2a) from the transfected cells, were collected and inoculated into Huh-7.5 cells to evaluate viral particle formation by measuring the luciferase activity (top). Results are shown as the mean values of triplicates $\pm$ SDs ($n = 3$ biological replicates). The expression levels of endogenous ANX5 and GAPDH were determined at 5 days postinoculation by IB (bottom). The Western blots are representative of three independent experiments.

Depletion of ANX5 does not affect cell proliferation. In general, the kinetics of viral spreading is dependent on cell proliferation. Therefore, we tested whether knockdown of ANX5 affects cell proliferation by performing a luminescent cell viability assay. The results showed that there was no significant difference in cell proliferation between the sh-NC and sh-ANX5 cells (Fig. 4A), suggesting that ANX5 is specifically involved in the negative regulation of HCV propagation.

ANX5 is not involved in HCV IRES-mediated translation. To investigate whether ANX5 is involved in HCV internal ribosome entry site (IRES)-mediated translation, we used a bicistronic reporter plasmid containing HCV IRESs derived from 1b (Con1) and 2a (JFH1) to monitor the activity of HCV IRES-mediated translation. Plasmids possessing the IRES sequence derived from poliovirus (PV) and encephalomyocarditis virus (EMCV) were used as controls. We observed no significant difference in any of the IRES-mediated reporter activities between sh-NC and sh-ANX5 cells (Fig. 4B), suggesting that ANX5 had no influence on HCV IRES-mediated translation.

ANX5 is not involved in HCV assembly. To investigate whether ANX5 is involved in HCV assembly, we used the *trans*-complemented HCV particle (HCVtcp) system, which produces an infectious HCV for single-round infection. A plasmid encoding core-
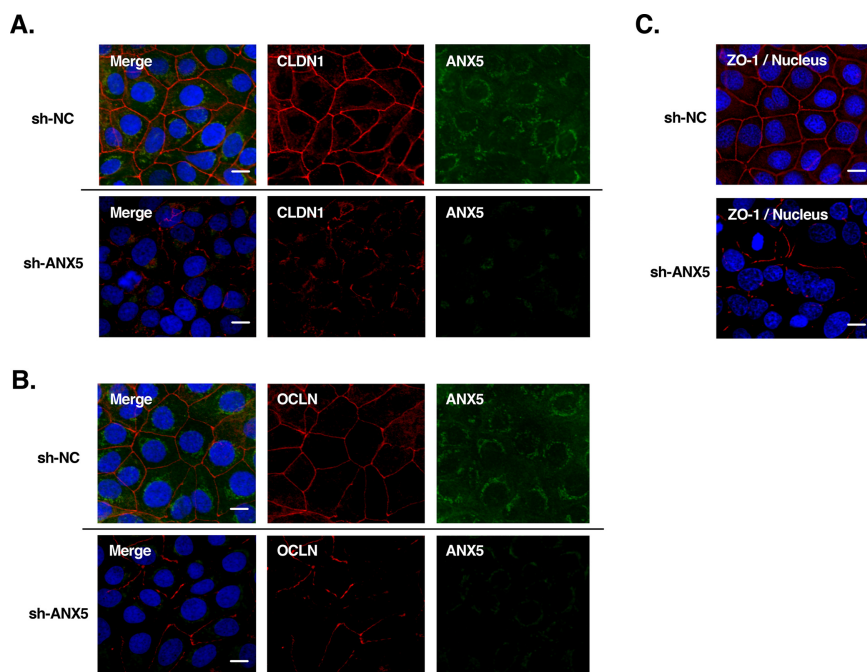
FIG 5 ANX5 is involved in regulation of the proper subcellular distribution of CLDN1 and OCLN. (A and B) Huh-7OK1-sh-NC and Huh-7OK1-sh-ANX5 cells were fixed with ice-cold acetone-methanol (1:1) solution for 20 min at −20°C and blocked with phosphate-buffered saline (PBS) containing 2% FBS for 1 h at room temperature. Endogenous CLDN1 (A) and endogenous OCLN (B) were stained with the specific mouse MAb together with ANX5 rabbit pAb, followed by staining with Alexa Fluor 594-conjugated goat anti-mouse IgG (red) and Alexa Fluor 488-conjugated goat anti-rabbit IgG (green), respectively. Nuclei were stained with Hoechst 33342. Scale bars, 10 μm. (C) Endogenous ZO-1 was stained with the specific mouse MAb, followed by staining with Alexa Fluor 594-conjugated goat anti-mouse IgG (red). Nuclei were stained with Hoechst 33342. Scale bars, 10 μm.

NS2 and a plasmid encoding a bicistronic subgenomic luciferase reporter replicon sequence were cotransfected into Huh-7.5 cells treated with siRNA-NC and siRNA-ANX5, respectively. At 5 days posttransfection, supernatants from the transfected cells were collected and inoculated into Huh-7.5 cells to evaluate viral particle formation by measuring the reporter activities. The results revealed that there was no significant difference in reporter activities between the siRNA-NC and siRNA-ANX5 cells (Fig. 4C), suggesting that ANX5 is not involved in HCV assembly. These results suggest that ANX5 participates in the negative regulation of the HCV life cycle, including viral replication and entry but not viral translation and assembly.

ANX5 is involved in regulation of cellular distribution of CLDN1 and OCLN. We observed that the expression levels of CLDN1 and OCLN were decreased in the ANX5 knockdown cells (Fig. 3B). Therefore, we hypothesized that ANX5 is involved in the regulation of cellular distribution of CLDN1 and OCLN. To test this hypothesis, we examined the intracellular localization of CLDN1 and OCLN by confocal microscopy. In sh-NC Huh-7OK1 cells, both CLDN1 and OCLN were distributed in a typical linear pattern along the layer of cell-to-cell contact (Fig. 5A and B, upper rows). Interestingly, cellular localization of CLDN1 and OCLN was severely disrupted and exhibited a fragmented and clumpy pattern in the sh-ANX5 Huh-7OK1 cells (Fig. 5A and B, lower rows). These results suggest that ANX5 is required for proper subcellular distribution of CLDN1 and OCLN. Similarly, ZO-1 protein, a scaffold protein of OCLN, was abnormally localized in the sh-ANX5 cells (Fig. 5C, lower image). These results suggest that ANX5 is involved in the regulation of subcellular distribution of CLDN1 and OCLN to maintain TJ assembly.

PKCη and PKCα are involved in both ANX5-mediated OCLN phosphorylation and OCLN assembly. To determine whether ANX5 is involved in PKC-mediated OCLN phosphorylation, we performed immunoblot analysis. The immunoblot analysis revealed that OCLN phosphorylation was markedly decreased in the sh-ANX5 cells compared with the sh-NC cells (Fig. 6A, first blot, compare lane 4 with lane 3). When we treated the
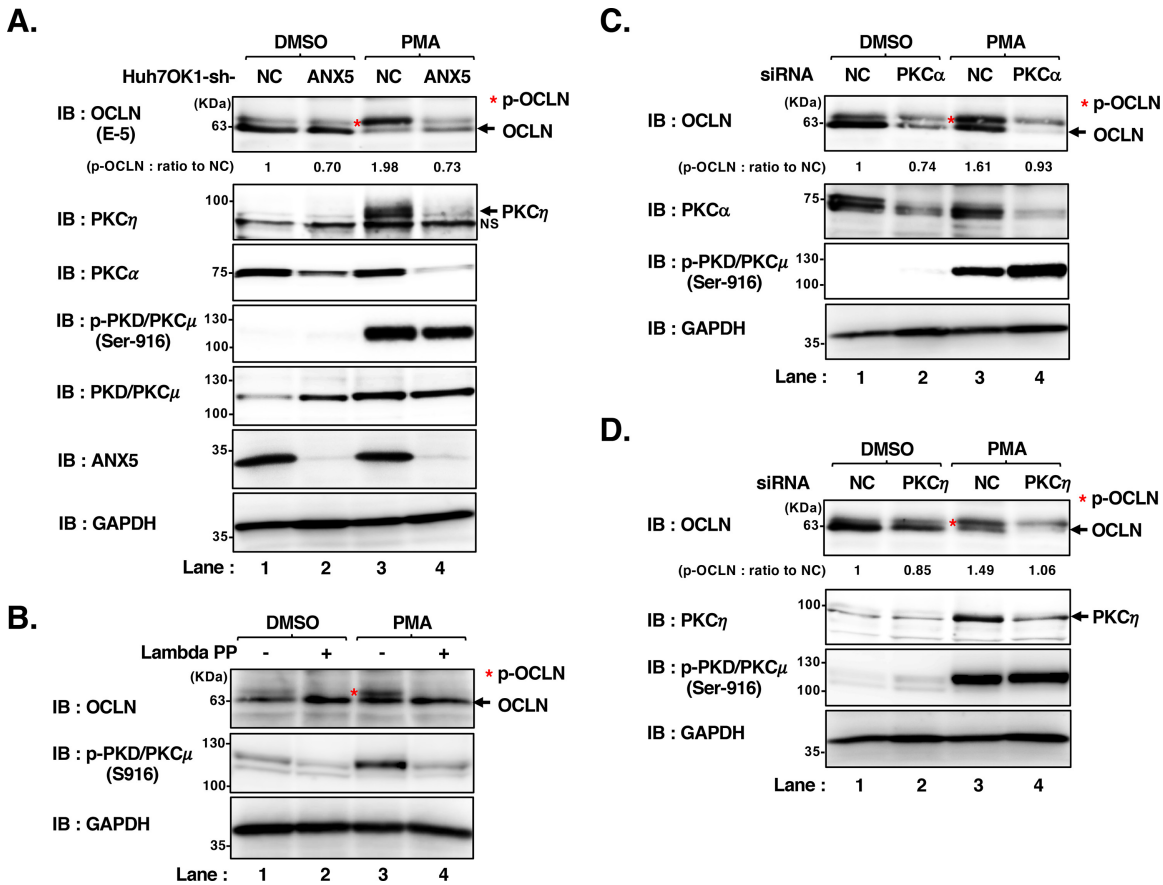
FIG 6 ANX5 regulates OCLN phosphorylation via induction of PKCη and PKCα expression. (A) Huh-7OK1-sh-NC and Huh-7OK1-sh-ANX5 cells were treated with dimethyl sulfoxide (DMSO) or 5 μg/mL of phorbol 12-myristate 13-acetate (PMA). At 3 h posttreatment, the cells were lysed and subjected to IB with the indicated antibodies. The asterisk indicates phosphorylated OCLN (p-OCLN). (B) Huh-7OK1 cells were treated with DMSO or 5 μg/mL of PMA. At 3 h posttreatment, the cells were lysed and treated with lambda PP for 30 min at 30°C. The samples were subjected to IB with the indicated antibodies. The asterisk indicates p-OCLN. (C and D) Huh-7OK1 cells were transfected with 50 nM synthetic siRNA targeted to NC, PKCη, or PKCα. At 3 days postincubation, the cells were treated with DMSO or 5 μg/mL of PMA for 3 h and subjected to IB with the indicated antibodies. The asterisk indicates p-OCLN. The Western blots are representative of three independent experiments. The relative levels of p-OCLN were quantified by ImageQuant TL software (version 7.0) and are indicated below the respective lanes.

cells with a PKC activator, phorbol 12-myristate 13-acetate (PMA), treatment with PMA clearly induced phosphorylation of OCLN protein (Fig. 6A, first blot, lane 3, asterisk). However, we could not detect clear phosphorylation of CLDN1 under the treatment with PMA (data not shown). Moreover, using antibodies to specific PKC isoforms, we observed marked decreases in the expression of PKCη and PKCα in the sh-ANX5 cells (Fig. 6A, second blot, lane 4, and third blot, lane 4), whereas phosphorylated PKD/PKCμ (Fig. 6A, fourth blot, lane 4) and other isoforms, including PKCδ, PKCζ, PKCθ, and PKCλ (data not shown), were not changed. These results suggest that ANX5 positively regulates OCLN phosphorylation via PKCη and PKCα expression. On the other hand, total PKD/PKCμ and phosphorylated PKD/PKCμ levels were comparable between the sh-NC and sh-ANX5 cells treated with PMA (Fig. 6A, lanes 3 and 4, fourth and fifth blots). We noticed that total PKD/PKCμ was moderately upregulated in the sh-ANX5 cells compared to sh-NC cells for undetermined reasons (Fig. 6A, fifth blot, compare lane 1 with lane 2).

To verify that the slowly migrating form of OCLN was due to phosphorylation, we performed experiments using lambda protein phosphatase (PP). When we treated the cells with lambda PP, the slowly migrating form of OCLN phosphorylation disappeared (Fig. 6B, top blot, compare lane 3 with lane 4, asterisks). The immunoblot analysis revealed that the phosphorylated PKD/PKCμ was also markedly decreased by the treatment of the cells with lambda PP (Fig. 6B, middle blot, compare lane 3 with lane 4).
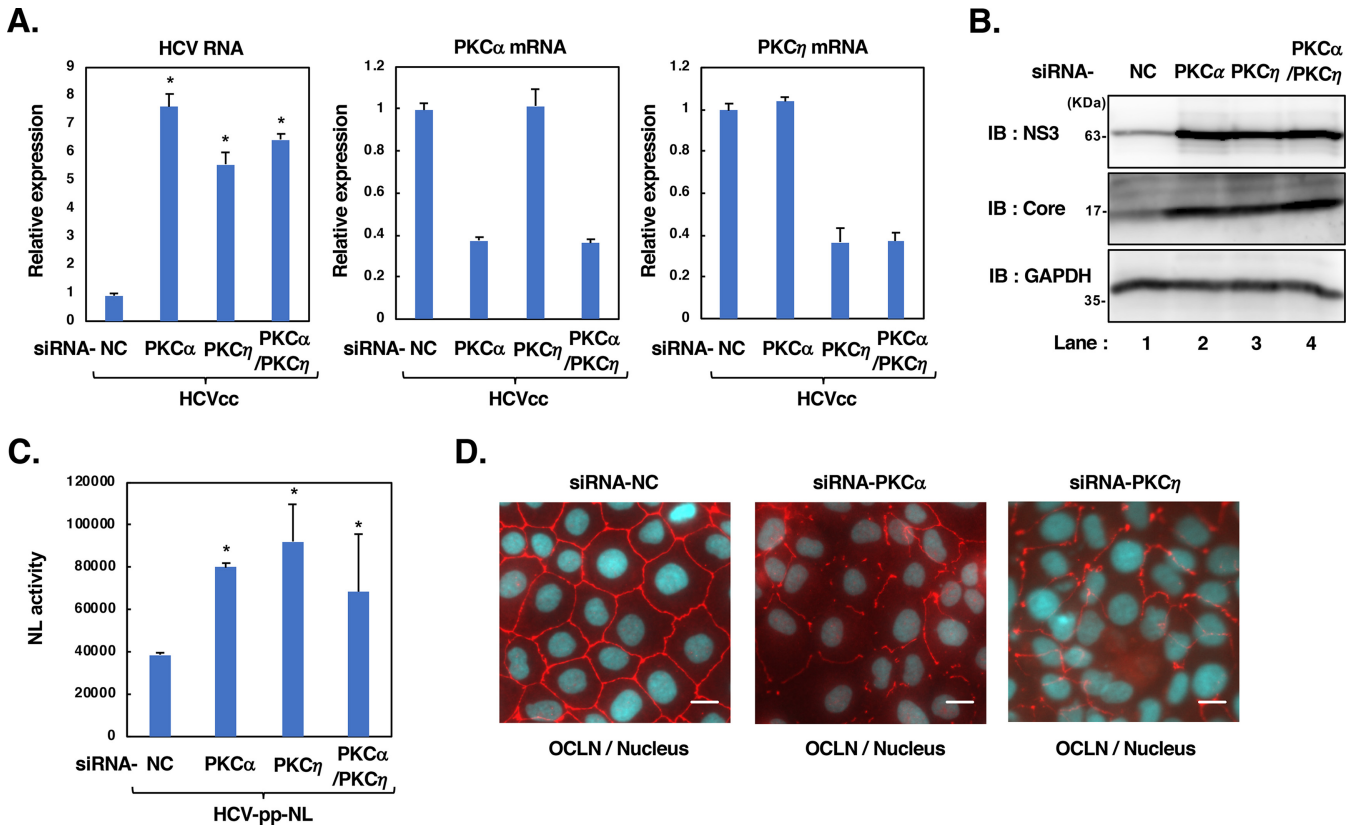
FIG 7 PKCη and PKCα are involved in the negative regulation of HCV propagation. (A and B) Huh-7OK1 cells were transfected with 50 nM synthetic siRNA targeted to the NC, PKCη, PKCα, or PKCη and PKCα. At 2 days posttransfection, the cells were infected with HCVcc J6/JFH1 at an MOI of 1. At 4 days postinoculation, cells were harvested. Total RNA was quantified by real-time PCR (A) with the indicated specific primers. The cell extracts were subjected to IB with the indicated antibodies (B). Results are the mean values of triplicates $\pm$ SDs. Data from the real-time PCR were normalized to the amount of GAPDH mRNA ($n = 3$ biological replicates). *, $P < 0.05$ versus the results for the HCVcc-infected Huh-7OK1 cells treated with siRNA-NC. (C) Huh-7OK1 cells were transfected with 50 nM synthetic siRNA targeted to NC, PKCη, or PKCα. At 3 days posttransfection, the cells were inoculated with HCVpps from genotype 1a (H77c), and the NL activity was measured at 3 days postinoculation. Results are the mean values of triplicates $\pm$ SDs ($n = 3$ biological replicates). *, $P < 0.05$ versus the results for the cells treated with siRNA-NC. (D) Huh-7OK1 cells were transfected with 50 nM synthetic siRNA targeted to NC, PKCη, or PKCα. At 3 days posttransfection, the cells were fixed with ice-cold acetone-methanol (1:1) solution for 20 min at $-20°C$ and blocked with PBS containing 2% FBS for 1 h at room temperature. Endogenous OCLN was stained with the specific mouse MAb, followed by staining with Alexa Fluor 594-conjugated goat anti-mouse IgG (red). Nuclei were stained with Hoechst 33342. Scale bars, 10 μm.

These results indicate that the slowly migrating form of OCLN was indeed the phosphorylated form of OCLN.

To further elucidate roles of PKCη and PKCα in ANX5-mediated OCLN phosphorylation, we performed siRNA-mediated knockdown experiments in the Huh-7OK1 cells. Immunoblot analysis revealed that PMA-induced OCLN phosphorylation was dramatically decreased by the knockdown of PKCη and PKCα (Fig. 6C and D, top blots, compare lane 3 with lane 4, asterisks). These results suggest that PKCη and PKCα are involved in ANX5-mediated OCLN phosphorylation.

PKCη and PKCα are involved in negative regulation of HCV propagation. To examine the role of PKCη and PKCα in HCV propagation, we evaluated the effects of siRNA-mediated knockdown of PKCη and PKCα on the HCV propagation. The knockdown efficiency for PKCη mRNA and PKCα mRNA was approximately 60% as estimated by qPCR (Fig. 7A, middle and right graphs). The qPCR analysis showed that PKCη mRNA was decreased by transfection of siPKCη but not transfection of siPKCα (Fig. 7A). In addition, PKCα was decreased by transfection of siPKCα but not transfection of siPKCη. These results validated the specificity of siPKCα and siPKCη. We observed significant enhancement of intracellular HCV RNA expression and intracellular HCV core protein and NS3 protein levels in both the PKCη knockdown and PKCα knockdown Huh-7OK1 cells to the same extent (Fig. 7A, left graph, and Fig. 7B, lanes 2 and 3). These results suggest that PKCη and PKCα are involved in negative regulation of HCV propagation. On the other
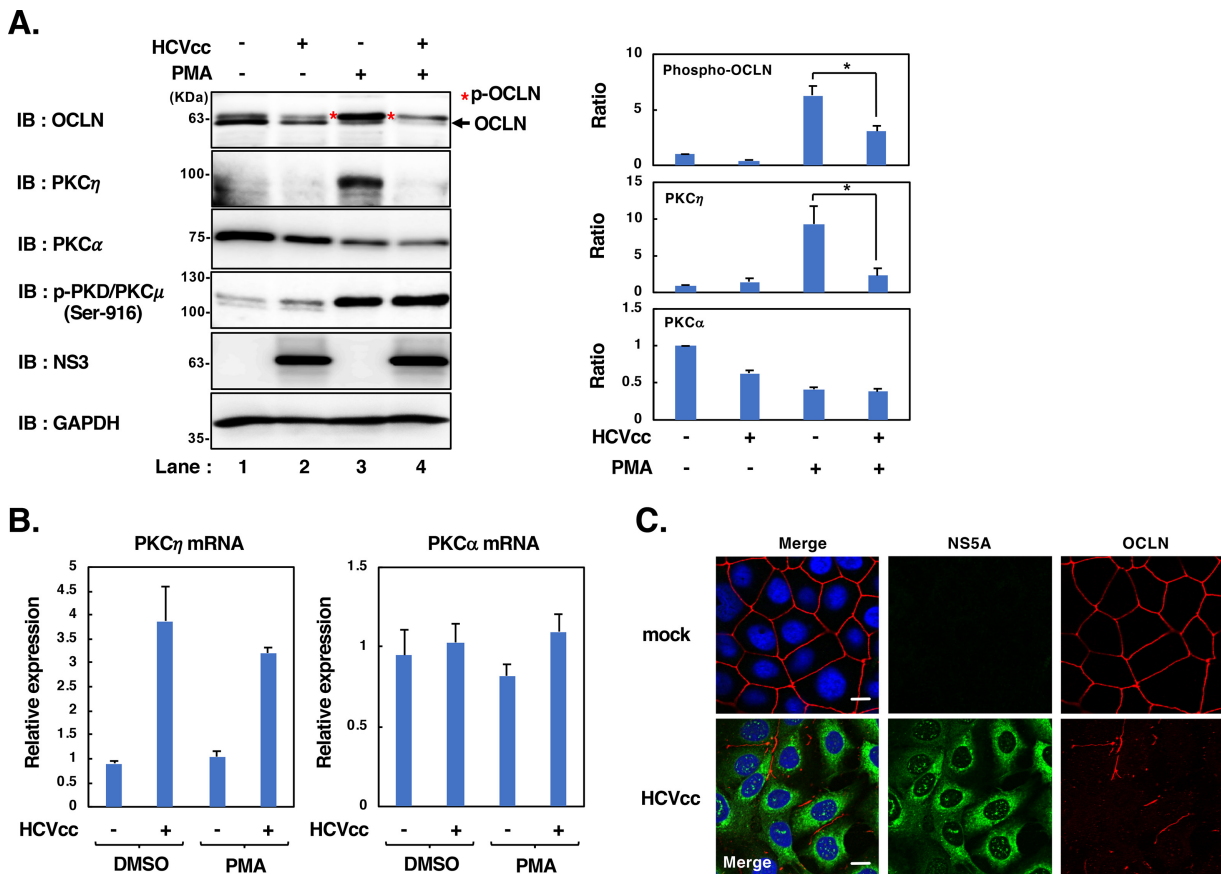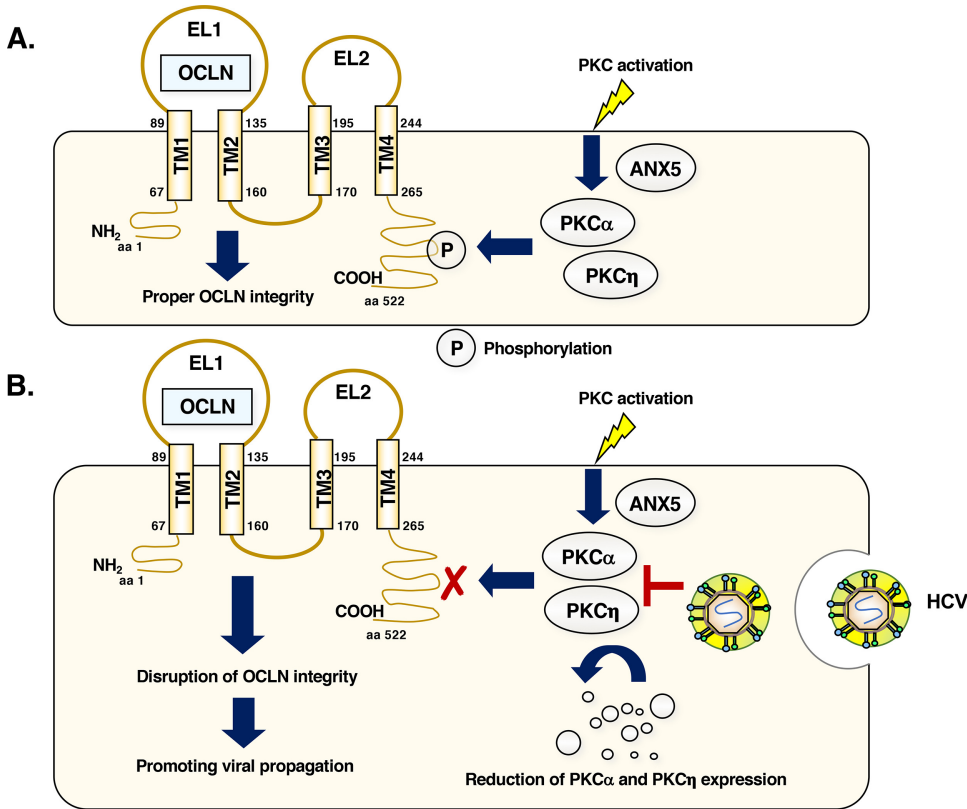
FIG 8 HCV infection disrupts OCLN integrity via downregulation of PKCα and PKCη expression, thereby promoting HCV propagation. (A) Huh-7OK1 cells were infected with HCVcc J6/JFH1 at an MOI of 1. At 3 days postinoculation, the cells were treated with 5 μg/mL of PMA for 3 h, harvested, and subjected to IB with the indicated antibodies. The asterisk indicates p-OCLN (left). The band intensities of phosphorylated OCLN, PKCη, and PKCα were determined by using ImageQuant TL software (version 7) (right). The Western blots are representative of three independent experiments. Results are the mean values of triplicates $\pm$ SDs ($n = 3$ biological replicates). *, $P < 0.05$ versus the results for the mock cells treated with PMA. (B) Huh-7OK1 cells were infected with HCVcc J6/JFH1 at an MOI of 1. At 3 days postinoculation, cells were treated with DMSO or 5 μg/mL of PMA for 3 h, and total RNA was quantified by real-time PCR with the primers for PKCη and PKCα. Results are the mean values of triplicates $\pm$ SDs. Data from the real-time PCR were normalized to the amount of GAPDH mRNA. (C) Huh-7OK1 cells were infected with HCVcc J6/JFH1 at an MOI of 1. At 4 days postinoculation, the cells were fixed and stained with anti-OCLN mouse MAb together with anti-NS5A rabbit pAb, followed by staining with Alexa Fluor 594-conjugated goat anti-mouse IgG (red) and Alexa Fluor 488-conjugated goat anti-rabbit IgG (green). Nuclei were stained with Hoechst 33342. Scale bars, 10 μm.

hand, the double knockdown of PKCα and PKCη showed neither an additive nor a synergistic effect on HCV propagation, suggesting that there is redundancy between PKCα and PKCη involving HCV infection (Fig. 7A, left graph, and Fig. 7B, lane 4).

Additionally, we observed that the infectivity of HCVpps was significantly enhanced in PKCη knockdown Huh-7OK1 cells, PKCα knockdown cells, and PKCα/PKCη double-knockdown cells (Fig. 7C). These results suggest that PKCη and PKCα are involved in negative regulation of HCV propagation at the HCV entry step.

To analyze the subcellular localization of OCLN in PKCη knockdown and PKCα knockdown Huh-7OK1 cells, we examined these cells under confocal microscopy. Confocal microscopy observation revealed that the knockdown of PKCα and PKCη disrupted subcellular localization of OCLN (Fig. 7D). These results suggest that PKCα and PKCη regulate OCLN localization and that PKCα and PKCη are involved in ANX5-mediated OCLN assembly.

HCV infection disrupts ANX5-mediated OCLN integrity via downregulation of PKCα and PKCη expression, thereby promoting HCV propagation. To further examine whether HCV disrupts ANX5-mediated OCLN integrity to promote viral infection, we assessed the effects of OCLN phosphorylation in HCVcc-infected cells. Immunoblot analysis revealed that HCV infection moderately decreased OCLN phosphorylation and PKCα protein levels in the cells (Fig. 8A, first and third blots, compare lane 1 with lane 2). We

FIG 9 A proposed model: HCV infection disrupts ANX5-mediated OCLN integrity mainly through downregulation of PKCα and PKCη expression, thereby promoting viral propagation. (A) Intracellular ANX5 regulates OCLN integrity via recruitment of PKCη and PKCα expression. PKCη and PKCα activation may be involved in OCLN phosphorylation at its C-terminal domain and contributes to the proper cellular distribution of OCLN. (B) HCV infects the cell via CD81 together with other viral entry factors, including CLDN1 and OCLN. Subsequently, HCV may reduce OCLN phosphorylation via downregulation of PKCα and PKCη expression, thereby promoting viral propagation via the disruption of OCLN integrity. HCV may promote degradation of PKCη by an undetermined mechanism.

also observed that HCV infection significantly decreased OCLN phosphorylation in cells treated with PMA (Fig. 8A, first blot, compare lane 3 with lane 4, asterisks). Intriguingly, PKCα protein level was reduced by HCV infection (Fig. 8A, third blot, compare lane 1 with lane 2), whereas the PMA-induced PKCη protein level was markedly reduced by HCV infection (Fig. 8A, second blot, compare lane 3 with lane 4), suggesting that HCV infection reduces OCLN phosphorylation via downregulation of PKCα and PKCη expression. The levels of phosphorylated PKD/PKCμ were not altered between mock-infected cells and HCV-infected cells (Fig. 8A, fourth blot, compare lane 3 with lane 4). On the other hand, the mRNA levels of PKCα and PKCη were not decreased in HCV-infected cells (Fig. 8B), suggesting that HCV downregulates PKCα and PKCη expression at the posttranslational level.

To investigate whether HCV infection disrupts OCLN distribution, we assessed the subcellular localization of OCLN in HCV-infected cells. Confocal microscopy analysis revealed that the proper subcellular distribution of OCLN was disrupted in HCV-infected cells (Fig. 8C).

Taken together, our findings lead us to propose a model that HCV infection disrupts ANX5-mediated OCLN assembly via downregulation of PKCα and PKCη expression to promote viral propagation (Fig. 9).

DISCUSSION

In this study, we demonstrated that ANX5 contributes to the suppression of HCV infection at the stages of viral entry and replication. We obtained evidence suggesting that ANX5 is involved in the regulation of OCLN distribution. Further mechanistic

analysis revealed that PKC isoforms, including PKCα and PKCη, are involved in ANX5-mediated OCLN integrity to restrict HCV infection. Furthermore, we found that HCV infection disrupts ANX5-mediated OCLN integrity through downregulation of PKCα and PKCη expression to promote viral infection. To our knowledge, the present study is the first to show a regulatory role of ANX5 in OCLN integrity to negatively control HCV infection.

Two independent studies using different purification analyses demonstrated that a set of three ANXs, i.e., ANX2, ANX4, and ANX5, were present in the HCV replication complex and may be associated with some HCV NS proteins (6, 7). In agreement with these observations, we demonstrated high expression of these three ANXs in Huh-7.5 cells (Fig. 1A). This result suggests the possibility that not only ANX2 but also ANX4 and ANX5 are involved in the HCV life cycle. On the other hand, Rösch and colleagues (9) reported that ANX3, which is enriched in lipid droplets (LDs), participates in HCV assembly, while ANX2, ANX4, and ANX5 did not show any impact on HCV infection. Our present findings demonstrated that knockdown of ANX5 also results in the enhancement of HCV RNA replication, although the molecular mechanism remains to be elucidated. We hypothesize that ANX5 may associate with the HCV replication complexes like ANX2 and ANX3 and negatively regulates HCV RNA replication. In light of these inconsistent reports, further investigation is needed to clarify the exact role of intracellular ANXs in the HCV life cycle.

Like other ANXs, ANX5 is highly associated with infections by several virus (e.g., cytomegalovirus [CMV], HIV-1, herpes simplex virus 1 [HSV-1], influenza A virus, vaccinia virus, and porcine reproductive and respiratory syndrome virus) (17–22). ANX5 is incorporated in the virion components and plays important roles in viral release. In the present study, we identified ANX5 as a host factor that negatively regulates the HCV life cycle at the stages of viral entry and replication. Knockdown of ANX5 exhibited neither cellular morphological changes nor alternation of cell growth (Fig. 4A), suggesting that ANX5-mediated HCV suppression is not due to the effects on host cell growth and cell arrest. Our present findings suggest that ANX5 is involved in the regulation of cellular distribution of CLDN1 and OCLN. A previous report by Mee and colleagues (16) indicated that HCV infectivity was facilitated by a disruption of CLDN1 and OCLN assembly. We thus propose a model that knockdown of ANX5 results in the enhancement of HCV infection through the disruption of CLDN1 and OCLN assembly (Fig. 9). Further investigation of the physiological association between ANX5 and TJ proteins, such as OCLN and CLDN1, is required to understand the mechanism underlying ANX5-mediated TJ assembly.

The association between the integrity of TJ proteins and ANX5 has not been reported. Our confocal microscopy analysis indicated that ANX5 was localized at perinuclear region near the sites of the HCV replication complex, while OCLN and CLDN1 were distributed at the cell-to-cell contact sites (Fig. 5A and B). These results suggest that ANX5 is involved the regulation of cellular distribution of CLDN1 and OCLN. In general, phosphorylation of OCLN and CLDN1 by several cellular kinases is associated with TJ assembly (15). Our results suggest that ANX5 is involved in the control of expression of specific PKC isoforms, such as PKCα and PKCη (Fig. 6A). Consistently, we observed the disruption of phosphorylation and subcellular distribution of OCLN in PKCα and PKCη knockdown cells (Fig. 6C and D and Fig. 7D). These results suggest that PKCα and PKCη function in both ANX5-mediated phosphorylation and assembly of OCLN and that ANX5 is involved in TJ assembly through the recruitment of PKCα and PKCη (Fig. 9A). On the other hand, it was reported that CLDN1 phosphorylation may be regulated by protein kinase A (PKA) (13), implicating the involvement of ANX5-mediated phosphorylation and distribution of CLDN1 via PKA activation.

Recently, Sekhar and colleagues (23) reported TACSTD2, a cell surface-expressed calcium-signaling receptor, as a host factor that associates with CLDN1 and OCLN and positively regulates their proper subcellular localization. Intriguingly, TACSTD2 knockdown disrupted TJ assembly and suppressed HCV infection. These results are inconsistent with our observation that disruption of CLDN1 and OCLN distribution promotes

HCV infection. Thus, it will be interesting to investigate the relationship between TACSTD2 and ANX5 and their roles in the regulation of TJ assembly.

We demonstrated that HCV disrupted ANX5-mediated OCLN assembly to promote viral infection, although HCV utilizes OCLN for the viral entry via cell-free or cell-to-cell infection. We also demonstrated that PKCη and PKCα are involved in ANX5-mediated OCLN phosphorylation and assembly (Fig. 6C and D and Fig. 7D). Intriguingly, HCV infection was associated with a moderate reduction of PKCα and a marked reduction of PMA-induced PKCη expression at the posttranslational level but not the transcriptional level (Fig. 8A and B). This result suggests that HCV manipulates OCLN assembly through downregulation of PKCα and PKCη to promote viral propagation (Fig. 9). However, further experiments are required to clarify how PKCα and PKCη expression is downregulated by HCV infection. Liu and colleagues (24) reported that HCV infection induces the downregulation of CLDN1 and OCLN expression to prevent superinfection, which suggests that cell-to-cell transmission rather than cell-free infection is involved in the persistent HCV infection. We demonstrated that HCV disrupts OCLN integrity via downregulation of PKCα and PKCη in HCV-infected cells. Thus, it will be interesting to determine whether cell-to-cell transmission is involved in the enhanced HCV propagation in cells with disrupted TJ assembly. Further investigation using the *ex vivo* organotypic three-dimensional (3D) culture model (25) is required to understand the role of ANX5-mediated TJ integrity and negative regulation of HCV infection in the liver.

In summary, we propose that HCV infection disrupts ANX5-mediated OCLN integrity through downregulation of PKCα and PKCη expression to promote viral propagation. Targeting the machinery of TJ disassembly by HCV infection may lead to the development of novel therapeutics for the treatment of HCV-related liver diseases.

MATERIALS AND METHODS

Cell culture and viruses. Huh-7.5 cells (kindly provided by C. M. Rice, The Rockefeller University, NY) and Huh-7OK1 cells (26) are highly permissive to the cell culture-adapted HCV (HCVcc) of genotype 2a strain JFH1. Huh-7.5 and Huh-7OK1 cells were maintained in Dulbecco's modified Eagle's medium (DMEM) (high glucose) with L-glutamine (Fujifilm Wako Pure Chemical Industries, Osaka, Japan) supplemented with 50 IU/mL of penicillin, 50 μg/mL of streptomycin (Gibco, Grand Island, NY), and 10% heat-inactivated fetal bovine serum (FBS; Biowest, Nuaillé, France) at 37°C in a 5% CO_2 incubator. The 9-13 cell line is an Huh-7 cell clone harboring the HCV SGR (1b, Con1) (27).

Cells were transfected with plasmid DNA using FuGene 6 transfection reagents (Promega, Madison, WI). The pFL-J6/JFH1 plasmid, which includes the entire viral genome of JFH1, a chimeric strain of HCV-2a (28), was kindly provided by C. M. Rice. The HCV genome RNA was synthesized *in vitro* using pFL-J6/JFH1 as a template and was transfected into Huh-7OK1 cells by electroporation. The virus produced in the culture supernatant was used for the infection experiments (29, 30).

Plasmids. The cDNA fragments including the IRES of the HCV strains derived from genotype 1b (Con1) or 2a (JFH1) were inserted between the *Renilla* and firefly luciferase genes, and the resulting plasmids were designated pRL-CMV-HCV/Con1 and pRL-CMV-HCV/JFH1, respectively (31). The IRES region of HCV was replaced with that of poliovirus (PV) or encephalomyocarditis virus (EMCV) and the resulting plasmids were designated pRL-CMV-PV and pRL-CMV-EMCV, respectively (31). The construction of an HCV reporter SGR plasmid including the firefly luciferase gene (pSGR-Luc) was kindly provided by R. Bartenschlager (Heidelberg University, Germany). The cDNA fragment encoding human ANX5 was amplified by reverse transcription-PCR (RT-PCR) from total RNA of Huh-7.5 cells and cloned into pEF1-Myc-His$_6$ using the In-Fusion HD cloning kit (Clontech, Mountain View, CA). The C-terminal Myc-His$_6$-tagged ANX5 wobble mutant (ANX5-shR) was generated by the mutagenesis PCR method using pEF1-ANX5-Myc-His$_6$ as a template. The sequences of the inserts were extensively confirmed by sequencing (Eurofins Genomics, Tokyo, Japan).

Antibodies and reagents. The mouse monoclonal antibodies (MAbs) used in this study were anti-core MAb (2H9 clone), anti-NS5A (MAB8694; Millipore, Billerica, MA), anti-NS3 (MAB8691; Millipore), anti-glyceraldehyde-3-phosphate dehydrogenase (anti-GAPDH) MAb (MAB374; Millipore), anti-ANX2 MAb (C-10; Santa Cruz Biotechnology, Santa Cruz, CA), anti-ANX4 MAb (D-2; Santa Cruz Biotechnology), anti-CLDN1 MAb (XX7; Santa Cruz Biotechnology), anti-OCLN MAb (E-5; Santa Cruz Biotechnology), anti-CLDN1 MAb (2H10D10; Thermo Scientific Inc., Waltham, MA), anti-CD81 MAb (BD Biosciences, San Jose, CA), and anti-β-actin MAb (Sigma-Aldrich, St. Louis, MO).

The rabbit polyclonal antibodies (pAbs) used in this study were anti-NS5A pAb (2914-1) (32), phospho-PKC antibody sampler pAb (number 9921; Cell Signaling Technology, Danvers, MA), anti-ANX5 pAb (14196; Abcam, Cambridge, UK), and anti-PKCη pAb (179524; Abcam). Horseradish peroxidase (HRP)-conjugated goat anti-mouse IgG and goat anti-rabbit IgG antibody (Molecular Probes, Eugene, OR) were used as secondary antibodies. Phorbol 12-myristate 13-acetate (PMA) was purchased from Sigma-Aldrich. Lambda protein phosphatase (lambda PP) was purchased from New England Biolabs, Inc. (Tokyo).

Immunoblot analysis. Cells were harvested and suspended in 0.5 mL of radioimmunoprecipitation assay (RIPA) buffer containing 50 mM Tris-HCl (pH 8.0), 150 mM NaCl, 0.1% sodium dodecyl sulfate (SDS), 1% NP-40, 0.5% deoxycholate (DOC), protease inhibitor cocktail tablets (Roche Molecular Biochemicals, Mannheim, Germany), and phosphatase inhibitor cocktail (Nacalai, Kyoto, Japan). Cell lysates were incubated at 4°C for 2 h and centrifuged at 20,400 × g for 30 min at 4°C (centrifuge MX-307 and rotor rack AR015-SC24; TOMY, Tokyo, Japan).

After being lysed, the samples were boiled in 15 μL of SDS sample buffer, then subjected to 8% or 10% SDS polyacrylamide gel electrophoresis (SDS-PAGE), and transferred to polyvinylidene difluoride (PVDF) membranes (Millipore). The membranes were blocked with Tris-buffered saline containing 20 mM Tris-HCl (pH 7.6), 135 mM NaCl, and 0.05% Tween 20 (TBST) plus 5% bovine serum albumin (BSA) at room temperature for 2 h and incubated with primary antibodies for immunoblotting. The membranes were then incubated with HRP-conjugated secondary antibody at room temperature for 2 h. The cell lysates were visualized with ECL Western blotting detection reagents (GE Healthcare, Buckinghamshire, UK) and detected by an LAS-4000 image analyzer system (GE Healthcare). The band intensities were quantified using ImageQuant TL software (version 7.0).

RNA interference. The siRNAs targeted to the human ANX2 (s1383), ANX4 (s1390), and ANX5 (s1392) were purchased from among *Silencer* select validated siRNAs (Thermo Scientific Inc.). HCV SGR (1b, Con1) cells were transfected with 50 nM siRNA using RNAiMax transfection reagent (Life Technologies, Carlsbad, CA) according to the manufacturer's instructions. At 72 h posttransfection, the cells were harvested and subjected to immunoblot analysis. The short hairpin RNA (shRNA) sequences of the sense strands targeted to human ANX5 (5′-GUACAUGACUAUAUCAGGA-3′) was inserted into the pSilencer 2.1 U6 puro vector (Ambion, Austin, TX). To establish the stable ANX5 knockdown cell clones, Huh-7OK1 cells were transfected with the plasmids, and drug-resistant clones were selected by treatment with puromycin (Sigma-Aldrich) at a final concentration of 1 μg/mL. The siRNAs targeted to the human PKCη (sense, 5′-GACAAGGACUUCAGUGUAAdTdT-3′; sense, 5′-GAACGAAGAUGACCUCUUUdTdT-3′; and sense, 5′-CCAUGGCACUAGAAAUAGUdTdT-3′) and PKCα (sense, 5′-AAAGGCUGAGGUUGCUGAUdTdT-3′) were purchased from Santa Cruz Biotechnology.

Real-time PCR. Total RNA was prepared from the cells using an RNeasy minikit (Qiagen, Valencia, CA). First-strand cDNA was synthesized using a GoScript reverse transcription system (Promega). Real-time PCR was performed using SYBR *Premix Ex Taq* II (Tli RNase H plus) (TaKaRa Bio, Shiga, Japan) according to the manufacturer's protocol. Fluorescent signals were analyzed by using a StepOne Plus real-time PCR system (Applied Biosystems Inc., Foster City, CA).

The following primer pairs were used to amplify the genes: for HCV, 5′-GAGTGTCGTGCAGCCTCCA (HCV-S)-3′ and 5′-CACTCGCAAGCACCCTATCA (HCV-AS)-3′; for ANX1, 5′-CGAAGTTGTGGATAGCTTCTGGTG (ANX1-S)-3′ and 5′-ACCGATCTGAGGACTTTGGTGTG (ANX1-AS)-3′; for ANX2, 5′-ACTTTGATGCTGAGCGGGATG (ANX2-S)-3′ and 5′-CGAAGGCAATATCCTGTCTCTGTG (ANX2-A)-3′; for ANX3, 5′-GAGTCACTAGGGCCACCATGAGA (ANX3-S)-3′ and 5′-GCGGCAGCTGATTGTTAAGGA (ANX3-AS)-3′; for ANX4, 5′-GAAGTGTGCCCGGATATCCAAC (ANX4-S)-3′ and 5′-GGTAGCTTTGAAGATGCTCTGCTG (ANX4-AS)-3′; for ANX5, 5′-GGTCTCTGCAAGGTAGGCAGGTA (ANX5-S)-3′ and 5′-AAACCATTGACCGCGAGACTTC (ANX5-AS)-3′; for ANX6, 5′-GCATCTGCGTCAGGGTTGAA (ANX6-S)-3′ and 5′-TCAGATGTGGGGAACTTAGTGCAGTG (ANX6-AS)-3′; for ANX7, 5′-GGGTAGCCACTACTTGGCACTT (ANX7-S)-3′ and 5′-CCCAACAGGCTACCCACCTT (ANX7-AS)-3′; for ANX9, 5′-GACAAGGATGCGCAGAGGCTA (ANX9-S)-3′ and 5′-GCTCCTGGAAGTTTCGTGAGATG (ANX9-AS)-3′; for ANX10, 5′-ATGATCCTGTGCAACAAGAGCTACC (ANX10-S)-3′ and 5′-CCAGCAGCTCCTGAAAGTATCCA (ANX10-AS)-3′; for ANX11, 5′-GCCTGATTGAGATCCTCGCTTC (ANX11-S)-3′ and 5′-AGTGCCCTGATGTGTCGCTTC (ANX11-AS)-3′; for ANX13, 5′-TTGAAATCTTATCGGGCAGGACA (ANX13-S)-3′ and 5′-TCGAAGTTTCCACTCAGCTCACTC (ANX13-AS)-3′; for PKCη, 5′-CATTTCGGCTCTCATGTTCCTCC (PKCη-S)-3′ and 5′-GCACATTCCGAAGTCTGCCAGT (PKCη-AS)-3′; for PKCα, 5′-GCCTATGGCGTCCTGTTGTATG (PKCα-S)-3′ and 5′-GAAACAGCCTCCTTGGACAAGG (PKCα-AS)-3′; and for GAPDH, 5′-GCCATCAATGACCCCTTCATT-3′ and 5′-TCTCGCTCCTGGAAGATGG-3′. The expression level of each gene was determined by the threshold cycle ($\Delta\Delta C_T$) method using GAPDH as an internal control.

Quantification of the extracellular core protein. HCV core protein in the culture supernatant was quantified by a highly sensitive enzyme immunoassay, the Ortho HCV core antigen enzyme-linked immunosorbent assay (ELISA; Ortho-Clinical Diagnostics, Raritan, NJ).

Flow cytometry. Cell surface expression of CD81 on Huh-7OK1-sh-NC and Huh-7OK1-sh-ANX5 cells was analyzed by flow cytometry (Becton, Dickinson, Mountain View, CA). Cells were incubated with mouse monoclonal antibody to CD81 (BD Biosciences) and then stained with the phycoerythrin (PE)-conjugated anti-mouse IgG monoclonal antibody (BD Biosciences). Mouse IgG1 was used as an isotype control.

HCV infectivity assay. Briefly, culture supernatants were serially diluted 10-fold and used to infect duplicate 24-well cultures of Huh-7.5 cells. At 24 h postinoculation, the cultures were overlaid with complete DMEM containing a final concentration of 0.25% methylcellulose (Sigma-Aldrich). At 72 h of incubation, the cells were fixed in 4% paraformaldehyde (PFA) and immunohistochemically stained using anti-core MAb (2H9 clone). The infectious HCV titers were determined based on the focus-forming units (FFU) per milliliter (29).

HCVpp infectivity assay. HCVpps were generated by cotransfection with a *gag-pol* packaging plasmid, a retroviral transfer vector carrying the nanoluciferase (NL) reporter gene, and a plasmid encoding viral envelope glycoprotein derived from HCV genotypes (1a, H77c; 1b, Con1; and 2a, JFH1) or VSV-G in HEK293T cells (33). The supernatants from the transfected cells were collected and inoculated into Huh-7OK1 cells to analyze the HCV infectivity.

HCVtcp assay. HCVtcps were generated as described previously (34). In brief, the plasmids encoding core-NS2 (pCAGC-NS2) and the plasmid encoding a bicistronic subgenomic luciferase reporter replicon sequence (SGR-Luc) were cotransfected into Huh-7.5 cells treated with siRNA-NC or siRNA-ANX5, respectively.

At 5 days posttransfection, supernatants from the transfected cells were collected and inoculated into Huh-7.5 cells to evaluate viral particle formation by measuring the luciferase reporter activity.

***In vitro* transcription of HCV RNA, electroporation into cells, and reporter analysis.** The HCV replicon plasmid pSGR (1b, Con1)-Luc was digested with ScaI and transcribed *in vitro* by using a MEGAscript T7 kit (Ambion). Then 10 μg of *in vitro*-transcribed HCV RNA was electroporated at 270 V and 960 μF by a GenePulser Xcells pulse generator (Bio-Rad, Hercules, CA) into 4×10^6 cells treated with BTXpress buffer (BTX, Holliston, MA). The electroporated cells were seeded into 24-well plates and harvested at the indicated time points. The luciferase activity was determined in triplicate using a GloMax 96 microplate luminometer (Promega). The luciferase activity at 4 h after electroporation was used for normalization for the transfection efficiency of HCV RNA.

Confocal microscopy. Cells seeded on glass coverslips in 24-well plates were infected or not with HCVcc J6/JFH1. At 5 days postinoculation, cells were fixed with ice-cold acetone-methanol (1:1) solution for 20 min at $-20°C$, stained with the appropriate antibodies, and then stained with Alexa Fluor 488- or Alexa Fluor 594-conjugated goat anti-mouse IgG (green) and Alexa Fluor 488- or Alexa Fluor 594-conjugated goat anti-rabbit IgG (red). Nuclei were stained with Hoechst 33342. The cells were mounted on glass slides and observed under a confocal laser scanning microscope (LSM700; Carl Zeiss, Oberkochen, Germany).

Statistics. Results are expressed as means $\pm$ standard deviations. Statistical significance was determined by Student's *t* test for results shown in Fig. 1D, Fig. 2A, C, and D, and Fig. 3B, C, and D and by one-way analysis of variance (ANOVA) for the results shown in Fig. 1C, Fig. 7A and C, and Fig. 8A. *P* values of <0.05 and <0.01 were considered significant.

REFERENCES

1. Moradpour D, Penin F. 2013. Hepatitis C virus proteins: from structure to function. Curr Top Microbiol Immunol 369:113–142. https://doi.org/10.1007/978-3-642-27340-7_5.
2. Moradpour D, Penin F, Rice CM. 2007. Replication of hepatitis C virus. Nat Rev Microbiol 5:453–463. https://doi.org/10.1038/nrmicro1645.
3. Lohmann V. 2013. Hepatitis C virus RNA replication. Curr Top Microbiol Immunol 369:167–198. https://doi.org/10.1007/978-3-642-27340-7_7.
4. Neufeldt CJ, Cortese M, Acosta EG, Bartenschlager R. 2018. Rewiring cellular networks by members of the Flaviviridae family. Nat Rev Microbiol 16:125–142. https://doi.org/10.1038/nrmicro.2017.170.
5. Harak C, Lohmann V. 2015. Ultrastructure of the replication sites of positive-strand RNA viruses. Virology 479–480:418–433. https://doi.org/10.1016/j.virol.2015.02.029.
6. Backes P, Quinkert D, Reiss S, Binder M, Zayas M, Rescher U, Gerke V, Bartenschlager R, Lohmann V. 2010. Role of annexin A2 in the production of infectious hepatitis C virus particles. J Virol 84:5775–5789. https://doi.org/10.1128/JVI.02343-09.
7. Saxena V, Lai CK, Chao TC, Jeng KS, Lai MM. 2012. Annexin A2 is involved in the formation of hepatitis C virus replication complex on the lipid raft. J Virol 86:4139–4150. https://doi.org/10.1128/JVI.06327-11.
8. Solbak SMO, Abdurakhmanov E, Vedeler A, Danielson UH. 2017. Characterization of interactions between hepatitis C virus NS5B polymerase, annexin A2 and RNA—effects on NS5B catalysis and allosteric inhibition. Virol J 14:236–403. https://doi.org/10.1186/s12985-017-0904-4.
9. Rösch K, Kwiatkowski M, Hofmann S, Schöbel A, Grüttner C, Wurlitzer M, Schlüter H, Herker E. 2016. Quantitative lipid droplet proteome analysis identifies annexin A3 as a cofactor for HCV particle production. Cell Rep 16:3219–3231. https://doi.org/10.1016/j.celrep.2016.08.052.
10. Gerke V, Moss SE. 2002. Annexins: from structure to function. Physiol Rev 82:331–371. https://doi.org/10.1152/physrev.00030.2001.
11. Koopman G, Reutelingsperger CP, Kuijten GA, Keehnen RM, Pals ST, Oers van MH. 1994. Annexin V for flow cytometric detection of phosphatidylserine expression on B cells undergoing apoptosis. Blood 84:1415–1420. https://doi.org/10.1182/blood.V84.5.1415.bloodjournal8451415.
12. Sawada N. 2013. Tight junction-related human diseases. Pathol Int 63:1–12. https://doi.org/10.1111/pin.12021.
13. French AD, Fiori JL, Camilli TC, Leotlela PD, O'Connell MP, Frank BP, Subaran S, Indig FE, Taub DD, Weerara AT. 2009. PKC and PKA phosphorylation affect the subcellular localization of claudin-1 in melanoma cells. Int J Med Sci 6:93–101. https://doi.org/10.7150/ijms.6.93.
14. Suzuki T, Elias BC, Seth A, Shen L, Turner JR, Giorgianni F, Desiderio D, Guntaka R, Rao R. 2009. PKC eta regulates occludin phosphorylation and epithelial tight junction integrity. Proc Natl Acad Sci U S A 106:61–66. https://doi.org/10.1073/pnas.0802741106.
15. Rao R. 2009. Occludin phosphorylation in regulation of epithelial tight junctions. Ann N Y Acad Sci 1165:62–68. https://doi.org/10.1111/j.1749-6632.2009.04054.x.
16. Mee CJ, Grove J, Harris HJ, Hu K, Balfe P, McKeating JA. 2008. Effect of cell polarization on hepatitis C virus entry. J Virol 82:461–470. https://doi.org/10.1128/JVI.01894-07.

17. Jensen ON, Houthaeve T, Shevchenko A, Cudmore S, Ashford T, Mann M, Griffiths G, Krijnse Locker J. 1996. Identification of the major membrane and core proteins of vaccinia virus by two-dimensional electrophoresis. J Virol 70:7485–7497. https://doi.org/10.1128/JVI.70.11.7485-7497.1996.

18. Varnum SM, Streblow DN, Monroe ME, Smith P, Auberry KJ, Pasa-Tolic L, Wang D, Camp DG, Rodland K, Wiley S, Britt W, Shenk T, Smith RD, Nelson JA. 2004. Identification of proteins in human cytomegalovirus (HCMV) particles: the HCMV proteome. J Virol 78:10960–10966. https://doi.org/10.1128/JVI.78.20.10960-10966.2004.

19. Chertova E, Chertov O, Coren LV, Roser JD, Trubey CM, Bess JW, Sowder RC, Barsov E, Hood BL, Fisher RJ, Nagashima K, Conrads TP, Veenstra TD, Lifson JD, Ott DE, Jr. 2006. Proteomic and biochemical analysis of purified human immunodeficiency virus type 1 produced from infected monocyte-derived macrophages. J Virol 80:9039–9052. https://doi.org/10.1128/JVI.01013-06.

20. Loret S, Guay G, Lippe R. 2008. Comprehensive characterization of extracellular herpes simplex virus type 1 virions. J Virol 82:8605–8618. https://doi.org/10.1128/JVI.00904-08.

21. Zhang C, Xue C, Li Y, Kong Q, Ren X, Li X, Shu D, Bi Y, Cao Y. 2010. Profiling of cellular proteins in porcine reproductive and respiratory syndrome virus virions by proteomics analysis. Virol J 7:242. https://doi.org/10.1186/1743-422X-7-242.

22. Berri F, Haffar G, Lê VB, Sadewasser A, Paki K, Lina B, Wolff T, Riteau B. 2014. Annexin V incorporated into influenza virus particles inhibits gamma interferon signaling and promotes viral replication. J Virol 88:11215–11228. https://doi.org/10.1128/JVI.01405-14.

23. Sekhar V, Pollicino T, Diaz G, Engle RE, Alayli F, Melis M, Kabat J, Tice A, Pomerenke A, Altan-Bonnet N, Zamboni F, Lusso P, Emerson SU, Farci P. 2018. Infection with hepatitis C virus depends on TACSTD2, a regulator of claudin-1 and occludin highly downregulated in hepatocellular carcinoma. PLoS Pathog 14:e1006916. https://doi.org/10.1371/journal.ppat.1006916.

24. Liu S, Yang W, Shen L, Turner JR, Coyne CB, Wang T. 2009. Tight junction proteins claudin-1 and occludin control hepatitis C virus entry and are downregulated during infection to prevent superinfection. J Virol 83:2011–2014. https://doi.org/10.1128/JVI.01888-08.

25. Baktash Y, Madhav A, Coller KE, Randall G. 2018. Single particle imaging of polarized hepatoma organoids upon hepatitis C virus infection reveals an ordered and sequential entry process. Cell Host Microbe 23:382–394.e5. https://doi.org/10.1016/j.chom.2018.02.005.

26. Okamoto T, Omori H, Kaname Y, Abe T, Nishimura Y, Suzuki T, Miyamura T, Yoshimori T, Moriishi K, Matsuura Y. 2008. A single-amino-acid mutation in hepatitis C virus NS5A disrupting FKBP8 interaction impairs viral replication. J Virol 82:3480–3489. https://doi.org/10.1128/JVI.02253-07.

27. Lohmann V, Korner F, Koch J, Herian U, Theilmann L, Bartenschlager R. 1999. Replication of subgenomic hepatitis C virus RNAs in a hepatoma cell line. Science 285:110–113. https://doi.org/10.1126/science.285.5424.110.

28. Lindenbach BD, Evans MJ, Syder AJ, Wölk B, Tellinghuisen TL, Liu CC, Maruyama T, Hynes RO, Burton DR, McKeating JA, Rice CM. 2005. Complete replication of hepatitis C virus in cell culture. Science 309:623–626. https://doi.org/10.1126/science.1114016.

29. Wakita T, Pietschmann T, Kato T, Date T, Miyamoto M, Zhao Z, Murthy K, Habermann A, Kräusslich H-G, Mizokami M, Bartenschlager R, Liang TJ. 2005. Production of infectious hepatitis C virus in tissue culture from a cloned viral genome. Nat Med 11:791–796. https://doi.org/10.1038/nm1268.

30. Bungyoku Y, Shoji I, Makine T, Adachi T, Hayashida K, Nagano-Fujii M, Ide Y-H, Deng L, Hotta H. 2009. Efficient production of infectious hepatitis C virus with adaptive mutations in cultured hepatoma cells. J Gen Virol 90:1681–1691. https://doi.org/10.1099/vir.0.010983-0.

31. Kukihara H, Moriishi K, Taguwa S, Tani H, Abe T, Mori Y, Suzuki T, Fukuhara T, Taketomi A, Maehara Y, Matsuura Y. 2009. Human VAP-C negatively regulates hepatitis C virus propagation. J Virol 83:7959–7969. https://doi.org/10.1128/JVI.00889-09.

32. Bawono RG, Abe T, Shibata Y, Matsui C, Deng L, Shoji I. 2021. NS5A-ISGylation via lysine 26 has a critical role for efficient propagation of hepatitis C virus genotype 2a. Kobe J Med Sci 67:E38–E47.

33. Shimizu Y, Shirasago Y, Kondoh M, Suzuki T, Wakita T, Hanada K, Yagi K, Fukasawa M. 2018. Monoclonal antibodies against occludin completely prevented hepatitis C virus infection in a mouse model. J Virol 92:e02258-17. https://doi.org/10.1128/JVI.02258-17.

34. Suzuki R, Saito K, Kato T, Shirakura M, Akazawa D, Ishii K, Aizaki H, Kanegae Y, Matsuura Y, Saito I, Wakita T, Suzuki T. 2012. Trans-complemented hepatitis C virus particles as a versatile tool for study of virus assembly and infection. Virology 432:29–38. https://doi.org/10.1016/j.virol.2012.05.033.